Article

Adsorption of Gases and Vapors on Nanoporous Ni(4,4‘-Bipyridine)(NO) Metal–Organic Framework Materials Templated with Methanol and Ethanol: Structural Effects in Adsorption Kinetics

Ashleigh J. Fletcher, Edmund J. Cussen, Darren Bradshaw, Matthew J. Rosseinsky, and K. Mark Thomas

J. Am. Chem. Soc., **2004**, 126 (31), 9750-9759• DOI: 10.1021/ja0490267 • Publication Date (Web): 20 July 2004

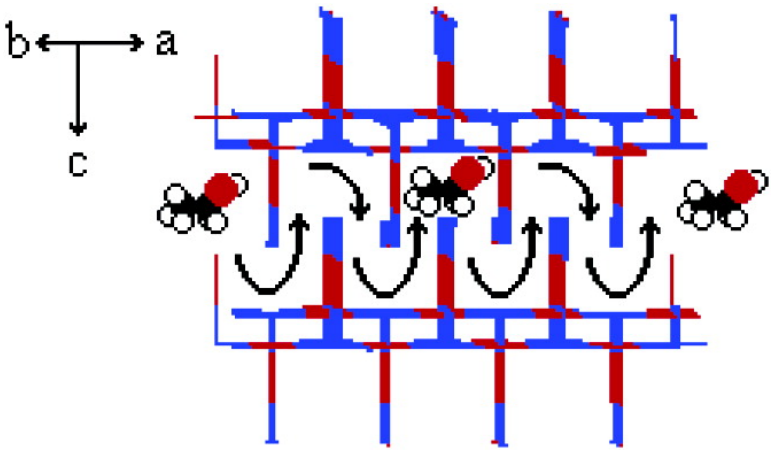

J|A|C|S
ARTICLES
Published on Web 07/20/2004

Adsorption of Gases and Vapors on Nanoporous $Ni_2(4,4'\text{-Bipyridine})_3(NO_3)_4$ Metal−Organic Framework Materials Templated with Methanol and Ethanol: Structural Effects in Adsorption Kinetics

Ashleigh J. Fletcher,[†] Edmund J. Cussen,[‡] Darren Bradshaw,[‡] Matthew J. Rosseinsky,[‡] and K. Mark Thomas*,[†]

Contribution from the Northern Carbon Research Laboratories, School of Natural Sciences, Bedson Building, University of Newcastle upon Tyne, Newcastle upon Tyne, NE1 7RU, U.K., and Department of Chemistry, University of Liverpool, Liverpool, L69 7ZD, U.K.

Received February 20, 2004; E-mail: mark.thomas@ncl.ac.uk

Abstract: Desolvation of $Ni_2(4,4'\text{-bipyridine})_3(NO_3)_4\cdot 2CH_3OH$ and $Ni_2(4,4'\text{-bipyridine})_3(NO_3)_4\cdot 2C_2H_5OH$ give flexible metal−organic porous structures **M** and **E**, respectively, which have the same stoichiometry, but subtly different structures. This study combines measurements of the thermodynamics and kinetics of carbon dioxide, methanol, and ethanol sorption on adsorbents **M** and **E** over a range of temperatures with adsorbent structural characterization at different adsorbate (guest) loadings. The adsorption kinetics for methanol and ethanol adsorption on porous structure **E** obey a linear driving force (LDF) mass transfer model for adsorption at low surface coverage. The corresponding adsorption kinetics for porous structure **M** follow a double exponential (DE) model, which is consistent with two different barriers for diffusion through the windows and along the pores in the structure. The former is a high-energy barrier due to the opening of the windows in the structure, required to allow adsorption to occur, while the latter is a lower-energy barrier for diffusion in the pore cavities. X-ray diffraction studies at various methanol and ethanol loadings showed that the host porous structures **E** and **M** underwent different scissoring motions, leading to an increase in unit cell volume with the space group remaining unchanged during adsorption. The results are discussed in terms of reversible adsorbate/adsorbent (host/guest) structural changes and the adsorption mechanism involving hydrogen-bonding interactions with specific surface sites for methanol and ethanol adsorption in relation to pore size and extent of filling. This paper contains the first evidence for individual kinetic barriers to diffusion through windows and pore cavities in flexible porous coordination polymer frameworks.

Introduction

Adsorbents have many important applications, including their use in catalysis or as catalyst supports, in gas separation and purification, and in environmental protection through pollution control and abatement.[1−3] Some adsorbents with well-established applications, such as activated carbons, are amorphous materials, and their pore structures may include a wide pore size distribution making the materials difficult to characterize precisely. However, there is considerable interest in adsorbents that have a well-defined crystalline structure, for example, alumnosilicates (zeolites) and aluminophosphates, and ordered mesoporous materials. Recently, crystalline porous materials based on metal−organic systems have been prepared in which the coordination polymer framework remains intact after removal of the solvent template/guest. These materials differ from other crystalline adsorbents in that they are flexible[4−7] and some have chiral properties.[8] Designing and tailoring materials with flexibility and well-defined porosity for chiral separations, ion exchange, gas storage, and catalytic applications represents a new development on the interface between coordination chemistry and materials science.

Highly porous and stable metal−organic framework materials containing guests have been prepared with multidentate ligands.[3−23] Ligand geometry controls the structure of the

[†] University of Newcastle upon Tyne.
[‡] University of Liverpool.

(1) Rouquerol, F.; Rouquerol, J.; Sing, K. *Adsorption by Powders and Porous Solids*; Academic Press: London, 1999.
(2) Barton, T. J.; Bull, L. M.; Klemperer, W. G.; Loy, D. A.; McEnaney, B.; Misono, M.; Monson, P. A.; Pez, G.; Scherer, G. W.; Vartuli, J. C.; Yaghi, O. M. *Chem. Mater.* **1999**, *11*, 2633.
(3) Yaghi, O. M.; Li, H.; Davis, C.; Richardson, D.; Groy, T. L. *Acc. Chem. Res.* **1998**, *31*, 474.
(4) Fletcher, A. J.; Cussen, E. J.; Prior, T. J.; Kepert, C. K.; Rosseinsky, M. J.; Thomas, K. M. *J. Am. Chem. Soc.* **2001**, *123*, 10001.
(5) Uemura, K.; Kitagawa, S.; Kondo, M.; Fukui, K.; Kitaura, R.; Chang, H.-C.; Mizutani, T. *Chem.-Eur. J.* **2002**, *8*, 3586.
(6) Kitaura, R.; Fujimoto, K.; Noro, S.-I.; Kondo, M.; Kitagawa, S. *Angew. Chem., Int. Ed.* **2002**, *41*, 133.
(7) Suh, M. P.; Ko, J. W.; Choi, H. J. *J. Am. Chem. Soc.* **2002**, *124*, 10976.
(8) Bradshaw, D.; Prior, T. J.; Cussen, E. J.; Claridge, J. B.; Rosseinsky, M. J. *J. Am. Chem. Soc.* **2004**, *126*, 6106.
(9) Eddaoudi, M.; Li, H.; Yaghi, O. M. *J. Am. Chem. Soc.* **2000**, *122*, 1391.
(10) Reineke, T. M.; Eddaoudi, M.; Fehr, M.; Kelley, D.; Yaghi, O. M. *J. Am. Chem. Soc.* **1999**, *121*, 1651.
(11) Reineke, T. M.; Eddaoudi, M.; Moler, D.; O'Keeffe, M.; Yaghi, O. M. *J. Am. Chem. Soc.* **2000**, *122*, 4843.
(12) Hoskins, B. F.; Robson, R. *J. Am. Chem. Soc.* **1990**, *112*, *1546*.
(13) Endo, K.; Koike, T.; Sawaki, T.; Hayashida, O.; Masuda, H.; Aoyama, Y. *J. Am. Chem. Soc.* **1997**, *119*, 4117.
(14) Kondo, M.; Yoshitomi, T.; Seki, K.; Matsuzaka, H.; Kitagawa, S. *Angew. Chem., Int. Ed. Engl.* **1997**, *36*, 1725.

10.1021/ja0490267 CCC: $27.50

network. Removal of the solvent from porous metal−organic framework materials may lead to the porous framework structure remaining intact, symmetry changes,[24] or pore volume collapse.[25] The design of guest-specific frameworks requires a detailed understanding of the sorption behavior of this class of crystalline nanoporous materials, and a limited number of studies of gas and vapor sorption on metal−organic framework materials have been reported.[4,11,25−28] A pore blocking process has been proposed on the basis of isotherm shapes at low relative pressure.[26] Molecular sieving and activated diffusion effects also need to be considered. The sorption process is complex especially in the cases where coordination may change, distortion of the host structure may occur to accommodate adsorbate molecules, and framework structural integrity may be compromised.

The main driving force for research on porous metal−organic framework materials has been the discovery of new materials with unique properties resulting from windows in the flexible porous structure. An improved knowledge of how different adsorbent structures arise from similar templates and how adsorbent structural characteristics influence the dynamic processes, by which the adsorbate diffuses into the adsorbent, is crucial for developing rational design strategies for these materials.

Porous metal−organic framework materials, with stoichiometry $Ni_2(4,4'\text{-bipyridine})_3(NO_3)_4$, prepared with methanol and ethanol as the template have subtly different structures, which maintain their framework structure after desolvation.[4,29,30] In this study, the adsorption characteristics of a series of gases and vapors on these two porous materials have been investigated to establish the influence of adsorbate structural factors on adsorption characteristics. These studies have been combined with X-ray diffraction studies of adsorbent/adsorbate structure at various stages of pore filling to establish structural changes during the adsorption process. The adsorption of guests with the same functional groups as the template, but different molecular size, into porous framework structures is compared to the adsorption characteristics of the templates used to form the structures.

Experimental Section

Materials Used. The porous framework materials used in this study, with formula $Ni_2(4,4'\text{-bipyridine})_3(NO_3)_4$, were prepared using methanol and ethanol templates as described previously.[29,30]

The gases used were supplied by BOC Ltd., London, U.K. and had the following purities: carbon dioxide (99.999%) and nitrogen (99.999%). Methanol (99.9%) and ethanol (99.9%) were obtained from Aldrich Chemicals, U.K.

Measurement of Adsorption Kinetics. The adsorption isotherm and kinetic measurements were carried out using an Intelligent Gravimetric Analyzer (IGA) supplied by Hiden Analytical Ltd., Warrington, U.K.[31] The instrument is an ultrahigh vacuum system with a fully computerized microbalance, which allows adsorption/desorption isotherms and the corresponding kinetics for each pressure increment to be determined, with the approach to equilibrium being monitored in real time using a computer algorithm.[32−38] The condition for achieving equilibrium was 99.9% of the predicted value calculated in real time by fitting the uptake profile to a stretched exponential kinetic decay model. The balance and pressure control systems were fully thermostated to ±0.2 K to eliminate the effects of changes in the external environment. The microbalance had a long-term stability of ±1 μg with a weighing resolution of 0.2 μg. The adsorbent sample (∼100 mg) was outgassed to a constant weight at 353 K and 10^{-5} Pa prior to measurement of the isotherms. The pressure was monitored by three pressure transducers with ranges of 0−0.2 kPa, 0−10 kPa, and 0−1 MPa. The liquid used to generate the vapor was degassed fully by repeated evacuation and vapor equilibration cycles of the liquid supply side of the vapor reservoir. The vapor pressure was gradually increased, over a timescale of ∼30 s to prevent disruption of the microbalance, until the desired value was achieved. The accuracy of the set-point pressure regulation was ±0.02% of the range used. The pressure was maintained at the set point by active computer control of inlet/outlet valves throughout the duration of the experiments. The sample temperature was measured at ∼5 mm from the sample and was controlled to ±0.05 K by circulation of a 1:1 mixture of ethylene glycol and water from a computer-controlled water bath. The initial pressure increment from high vacuum ($<10^{-5}$ Pa) resulted in a change of sample temperature of ∼0.5 K due to the introduction of conduction from the thermostatically controlled water jacket through the gas to the sample. The isotherms were typically repeatable to better than ±1%.

The saturated vapor pressures were calculated using the following equation[39,40]

$$\log_{10} p = A - \frac{B}{T + C} \tag{1}$$

where p is the saturated vapor pressure (Torr), T is the temperature in degrees Celsius, and A, B, and C are constants defined by the adsorbate: methanol (259−338 K), $A = 7.89750$, $B = 1474.08$, $C = 229.13$; ethanol (271−373 K), $A = 8.32109$, $B = 1718.10$, $C = 237.52$; carbon dioxide (77−303 K), $A = 7.810237$, $B = 995.7048$, $C = 293.4754$.

X-ray Diffraction Measurements. X-ray diffraction experiments were performed on samples of partially loaded porous framework material in sealed Lindeman capillaries. The samples were prepared by outgassing Lindemann tubes at 10^{-5} Pa and 353 K for 24 h using an IGA system. The material was loaded with methanol or ethanol vapor at 293 K at various relative pressures (p/p^0) with computer-controlled pressure setting. Powder diffraction data were recorded in the angular range $5° \leq 2\theta \leq 30°$ on a Stoe Stadi-P diffractometer with

(15) Venkataraman, D.; Gardner, G. B.; Lee, S.; Moore, J. S. *J. Am. Chem. Soc.* **1995**, *117*, 11600.
(16) Zaworotko, M. J. *Chem. Commun.* **2001**, *1*, 1.
(17) Li, H.; Laine, A.; O'Keeffe, M.; Yaghi, O. M. *Science* **1999**, *283*, 1145.
(18) Gardner, G. B.; Venkataraman, D.; Moore, J. S.; Lee, S. *Nature* **1995**, *374*, 792.
(19) Li, H.; Eddaoudi, M.; Groy, T. L.; Yaghi, O. M. *J. Am. Chem. Soc.* **1998**, *120*, 8571.
(20) Yaghi, O. M.; Li, H.; Groy, T. L. *Inorg. Chem.* **1997**, *36*, 4292.
(21) Seo, J. S.; Whang, D.; Lee, H.; Jun, S. I.; Oh, J.; Jeon, Y. J.; Kim, K. *Nature* **2000**, *404*, 982.
(22) Eddaoudi, M.; Moler, D. B.; Li, H.; Chen, B.; Reineke, T. M.; O'Keeffe, M.; Yaghi, O. M. *Acc. Chem. Res.* **2001**, *34*, 319.
(23) James, S. L. *Chem. Soc. Rev.* **2003**, *32*, 276.
(24) Kepert, C. J.; Hesek, D.; Beer, P. D.; Rosseinsky, M. J. *Angew. Chem., Int. Ed.* **1998**, *37*, 3158.
(25) Li, D.; Kaneko, K. *Chem. Phys. Lett.* **2001**, *335*, 50.
(26) Li, D.; Kaneko, K. *J. Phys. Chem. B* **2000**, *104*, 8940.
(27) Kepert, C. J.; Prior, T. J.; Rosseinsky, M. J. *J. Am. Chem. Soc.* **2000**, *122*, 5158.
(28) Kondo, M.; Shimamura, M.; Noro, S.-I.; Minakoshi, S.; Asami, A.; Seki, K.; Kitagawa, S. *Chem. Mater.* **2000**, *12*, 1288.
(29) Kepert, C. J.; Rosseinsky, M. J. *Chem. Commun.* **1999**, 375.
(30) Cussen, E. J.; Claridge, J. B.; Rosseinsky, M. J.; Kepert, C. J. *J. Am. Chem. Soc.* **2002**, *124*, 9574.
(31) Benham, M. J.; Ross, D. K. *Z. Phys. Chem.* **1989**, *163*, 25.
(32) Reid, C. R.; O'koye, I. P.; Thomas, K. M. *Langmuir* **1998**, *14*, 2415.
(33) Reid, C. R.; Thomas, K. M. *Langmuir* **1999**, *15*, 3206.
(34) Harding, A. W.; Foley, N. J.; Norman, P. R.; Francis, D. C.; Thomas, K. M. *Langmuir* **1998**, *14*, 3858.
(35) O'koye, I. P.; Benham, M.; Thomas, K. M. *Langmuir* **1997**, *13*, 4054.
(36) Foley, N. J.; Thomas, K. M.; Forshaw, P. L.; Stanton, D.; Norman, P. R. *Langmuir* **1997**, *13*, 2083.
(37) Fletcher, A. J.; Thomas, K. M. *Langmuir* **1999**, *15*, 6908.
(38) Fletcher, A. J.; Thomas, K. M. *Langmuir* **2000**, *16*, 6253.
(39) *Lange's Handbook of Chemistry*, 15th ed.; McGraw-Hill: New York, 1999.
(40) CRC *Handbook of Chemistry and Physics*, 74th ed.; CRC Press: Boca Ratan, FL, 1993.

a linear position sensitive detector and monochromatic Cu $K_{\alpha 1}$ radiation from a germanium monochromator.

Results and Discussion

Porous Structures. Ni_2(4,4′-bipyridine)$_3$$(NO_3)_4$ forms structures with a range of solvents as guests in the framework: for example, methanol, ethanol, chlorobenzene, *o*-dichlorobenzene, benzene, nitrobenzene, toluene or anisole,[41] carbon disulfide, and water.[15,42,43] The porous structures prepared using methanol and ethanol as templates are designated as **M** and **E**, respectively, and are shown in Figure 1a and b. Both structures have the same stoichiometry and contain Ni-bipy linear chains linked together, with T-shaped bipy coordination at the metal, into pairs. These pairs are aligned parallel to each other in the "ladder" structure of **M** and perpendicular in the "tongue and groove" structure of **E**.

Porous structure **E** consists of a unidirectional set of nonintersecting linear arrays of cavities (5.4 × 5.2 × 4.1 Å) with connecting windows.[29] The channels are not interconnected and are predominantly lined by the π-systems of the 4,4′-bipyridine ligands. The windows in the pore structure may be defined by approximately perpendicular dimensions between 2 oxygen atoms from nitrate groups (2.32 Å) and 2 hydrogen atoms in the 2 position on the 4,4′-bipyridine ligands (2.75 Å).[4] The noncoordinating oxygen atom from each nitrate group is hydrogen bonded (50% occupancy) to the hydroxyl group of the ethanol guest. However, the crystal structure has quite large displacement parameters for the nitrate and 4,4′-bipyridine (which rocks about the C2 axis defined by the 1 and 4 positions on the ring).

Porous structure **M** comprises a ladder arrangement of Ni centers with hydrogen bonding between the ladders.[30] The 4,4′-bipyridines of the infinite chains are disordered about the C2 axis. There is evidence for positional disorder of the noncoordinating oxygen atoms of the nitrates. The larger pores are linked by rectangular-shaped windows, the size of which is influenced by disorder with maximum dimensions 2.5 × 4.9 Å, predominantly in the *b* and *a* dimensions, respectively. The pore cavities (4.3 × 5.3 × 8.3 Å) in **M** are predominantly lined by the π-systems of the 4,4′-bipyridine ligands, hydrogen atoms, and the noncoordinating oxygen atoms of the nitrate groups, as in the case of **E**. The methanol molecules are disordered in Ni_2-(4,4′-bipyridine)$_3$$(NO_3)_4$·$2CH_3OH$ and cannot be located crystallographically. The results from PLATON give a solvent-accessible volume of 1840 Å^3 for the unit cell (23.1% of the total cell volume) of the as-made material, **M**. There are eight Ni_2 formula units per cell, which gives a free volume of 230 Å^3 per dimer. If we take the two methanol molecules to have a volume of 134.2 Å^3 (see ref 26), this gives pore filling of 58.4% of the total space available. Methanol is readily lost from the "as-grown" crystal. This is consistent with the crystallographic results, which indicate only partial pore filling.

The void volumes calculated from the crystallographic data for **M** and **E** indicate that the smaller template gives the larger pore volume (×1.335). The windows in **M** and **E** are clearly too small for methanol (3.81 × 4.18 × 4.95 Å) and ethanol (4.16 × 4.27 × 6.33 Å)[44,45] to pass through without distorting the structure around the window. Crystallographic information for both structures is provided in the Supporting Information.

Adsorption Isotherms. In this paper, the term pressure increment is used to describe pressure changes used to generate the isotherm, whereas isotherm steps refer to changes in isotherm shape. Carbon dioxide studies involve adsorption on nonspecific surface sites, whereas methanol and ethanol adsorption takes place by hydrogen bonding to specific surface sites.

Carbon Dioxide Adsorption Isotherms. Carbon dioxide adsorption isotherms for **E** and **M** at 273 K are shown in Figure 2. There is a step in the isotherm for **E** at low relative pressure ($p/p^0 \approx 0.001-0.002$). In contrast, the carbon dioxide adsorption isotherm for **M** was Type I and showed no evidence of any steps in the isotherm.

The adsorption characteristics of adsorptives on microporous materials can be compared using the Dubinin−Radushkevich (D−R) equation:

$$\log n = \log n_0 - D \log^2(p^0/p) \qquad (2)$$

where n is the amount adsorbed at a given pressure p, n_0 is the amount adsorbed corresponding to the micropore volume, p^0 is the saturated vapor pressure, and D is a constant related to the microporous structure of the adsorbent.[46] Estimates of the micropore volumes from carbon dioxide adsorption on **E** at 273 K, both before and after the isotherm steps, were obtained using the D−R graphs. The values were 0.119 and 0.098 cm^3 g^{-1} for before and after the step, respectively, while the total pore volume based on methanol and ethanol adsorption was 0.149 cm^3 g^{-1}. The corresponding results for carbon dioxide adsorption on **M** at 273 K gave a micropore pore volume of 0.113 cm^3 g^{-1}, while the pore volume derived from crystallographic void information was ∼0.166 cm^3 g^{-1}. It is apparent that the estimated micropore volumes obtained from D−R graphs must be used with caution.

Methanol and Ethanol Adsorption Isotherms. Adsorption isotherms for methanol and ethanol on **E** at 293 K are shown in Figure 3a. The ethanol isotherm is Type I in the IUPAC classification scheme and shows a steep uptake at low relative pressure. In contrast, the methanol adsorption isotherm is less steep at low relative pressure. Previous studies have shown that a step exists in the isotherm at ∼70% loading at low temperature.[4] This has been attributed to structural change resulting from the occupation of all surface nitrate sites available for hydrogen bonding and the need for structural change to accommodate additional adsorbate molecules. The total pore volumes obtained from methanol and ethanol adsorption isotherms on **E** were ∼0.148 and ∼0.149 cm^3 g^{-1}, respectively. The total pore volume calculated from the stoichiometry determined using crystallographic data for Ni_2(4,4′-bipyridine)$_3$-$(NO_3)_4$·$2C_2H_5OH$ was 0.142 cm^3 g^{-1}. The slightly larger (4−5%) uptake, than the stoichiometry obtained from the X-ray crystallographic studies, is attributed to defects in the structure of the material.

(41) Moulton, B.; Zaworotko, M. J. *Chem. Rev.* **2001**, *101*, 1629.
(42) Biradha, K.; Mondal, A.; Moulton, B.; Zaworotko, M. J. *Dalton* **2000**, *21*, 3837.
(43) Power, K. N.; Hennigar, T. L.; Zaworotko, M. J. *New J. Chem.* **1998**, *22*, 177.
(44) Webster, C. E.; Drago, R. S.; Zerner, M. C. *J. Am. Chem. Soc.* **1998**, *120*, 5509.
(45) Webster, C. E.; Zerner, M. C. (Private Communication calculated by the methods described in ref 44).
(46) Dubinin, M. M. In *Characterization of Porous Solids*; Sing, K. S. W., Ed.; Society of Chemical Industries: London, 1979; Vol. 1, pp 1−11.

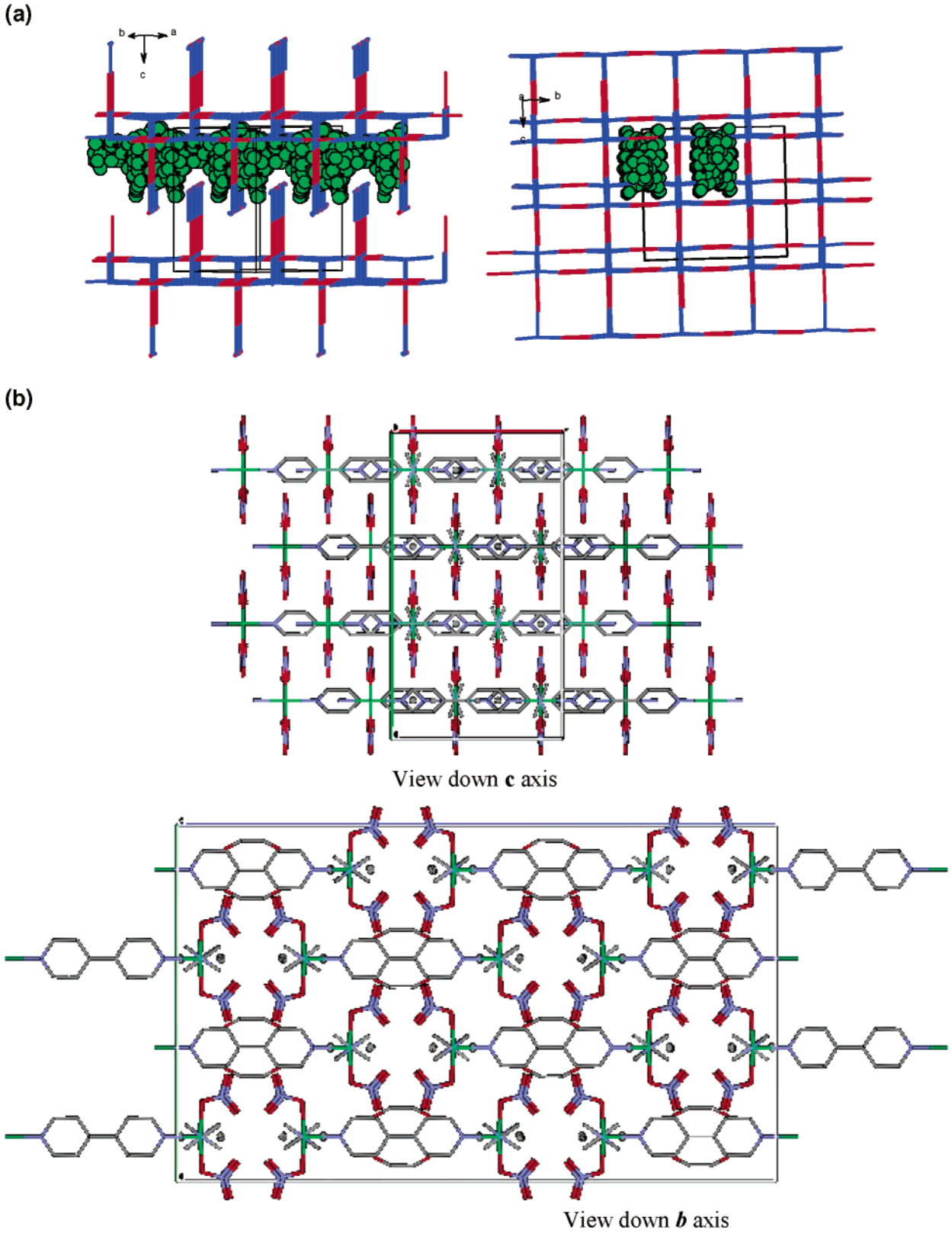

Figure 1. (a) Structure of **E** (ethanol-templated $Ni_2(4,4'\text{-bipyridine})_3(NO_3)_4$). (b) Structure of **M** (methanol-templated $Ni_2(4,4'\text{-bipyridine})_3(NO_3)_4$ with methanol molecules removed).

The adsorption of methanol on **M** has an isotherm with a shape similar to that obtained for adsorption of methanol on **E**. However, there is no evidence for steps in the isotherm of the former. The total pore volume obtained from extrapolation of the isotherm data to $p/p^0 = 1$, which gave a methanol uptake of ~4.48 mmol g^{-1} (see Figure 3b), was 0.181 $cm^3\ g^{-1}$, assuming an adsorbate density of 0.7914 g cm^{-3}. This compares with a pore volume predicted from the void volume of the

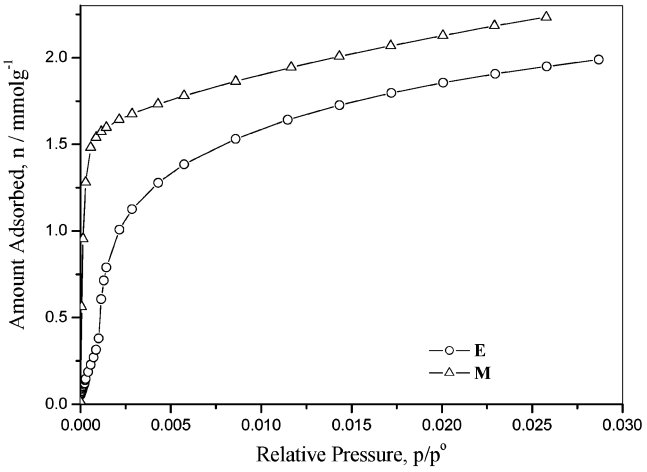

Figure 2. Isotherms for carbon dioxide adsorption on porous structures **M** (△) and **E** (○) at 273 K.

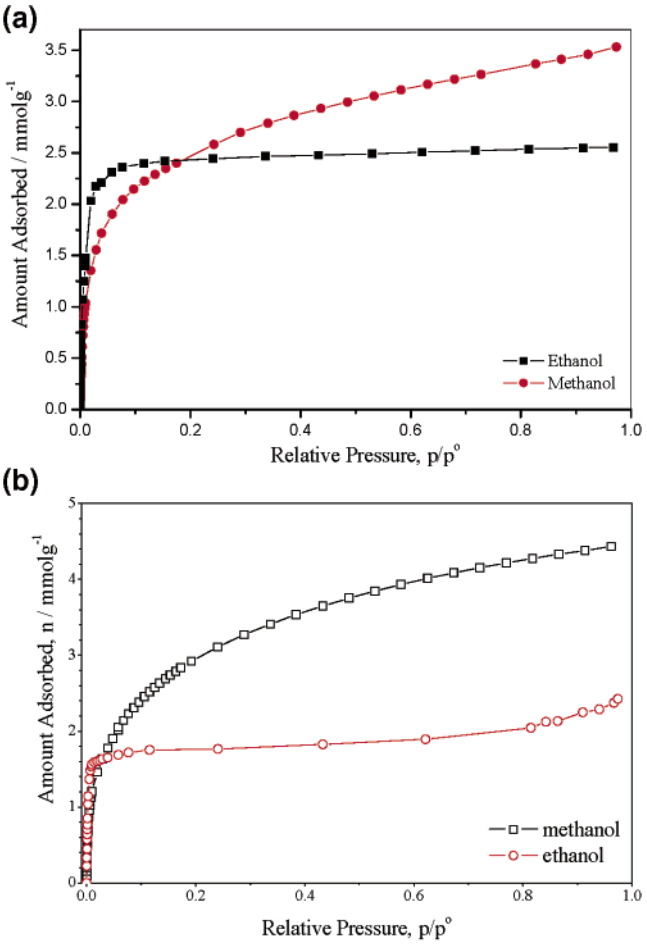

Figure 3. (a) A comparison of the adsorption isotherms for methanol and ethanol on porous structure **E** at 298 K. (b) A comparison of the adsorption isotherms for methanol at 273 K and ethanol at 298 K on porous structure **M**.

crystallographic data for $Ni_2(4,4'\text{-bipyridine})_3(NO_3)_4 \cdot 2CH_3OH$ of 0.166 $cm^3\ g^{-1}$, while the actual amount of methanol based on stoichiometry corresponds to 0.097 $cm^3\ g^{-1}$.

The adsorption of ethanol on **M** is quite different, having a steep uptake at low relative pressure with a shallow plateau region (1.7−2.0 mmol g^{-1}) over the relative pressure range $p/p^0 = 0.1-0.8$. The uptake at $p/p^0 = 1$ was ∼2.42 mmol g^{-1}, and the amount adsorbed corresponds to a pore volume of 0.141 $cm^3\ g^{-1}$ assuming that the density of adsorbed ethanol is 0.7893 g cm^{-3}. This is considerably lower than the pore volume (0.181 $cm^3\ g^{-1}$) obtained from methanol adsorption, indicating incomplete pore filling. This can be attributed to the stability of specific hydrogen-bonded interactions, between the adsorbate and surface sites in **M**.

Adsorption Thermodynamics. Hysteresis for the adsorption/desorption of methanol on **M** is insignificant. The isosteric enthalpies (ΔH_i) and entropies (ΔS_i) of adsorption were calculated at constant surface coverage using the following equation:

$$\ln(p) = \Delta H_i/RT - \Delta S_i/R \qquad (3)$$

where p is the pressure, R is the gas constant, and T (K) is the temperature.[1] The values of ΔH_i and ΔS_i obtained for methanol adsorption on **M** over the temperature range 268−288 K were 61−65 kJ mol^{-1}. These values are similar to the values obtained for both methanol and ethanol adsorption on **E**.[4] The methanol adsorption isotherms for **E** give values for ΔH_i that do not change markedly until ∼70% loading (pore volume ≈ 0.11 $cm^3\ g^{-1}$) where the step in the isotherm and the slow adsorption kinetics are observed.[4] This is consistent with methanol initially filling the sites occupied by ethanol. The ΔH_i values are similar to those obtained for the adsorption of ethanol and methanol on active carbons.[38]

Adsorption Kinetics. Linear driving force (LDF), combined barrier resistance/Fickian diffusion (CBRD),[32,33,37,38,47] and Fickian models[33,48] provide satisfactory descriptions, in most cases, of the adsorption kinetics of various gases/vapors on carbon molecular sieves and activated carbons, depending on the adsorptive and experimental conditions used. The LDF model is described by the following equation:

$$M_t/M_e = 1 - \exp(-kt) \qquad (4)$$

where M_t is the mass uptake at time t, M_e is the mass uptake at equilibrium, and k is the kinetic rate constant. The LDF model is consistent with a single rate constant (k), relaxation time, and barrier to diffusion into the porous structure. The LDF rate constants for adsorption of methanol and ethanol on **E** decrease with increasing relative pressure in the low relative pressure region. Methanol adsorption on **E** deviates from the LDF model at $p/p^0 > 0.048$ (uptake ∼2 mmol g^{-1} or ∼50% total pore volume), while ethanol adsorption deviates at $p/p^0 > 0.078$ (uptake ∼2.3 mmol g^{-1} or ∼90% total pore volume). The CBRD model is obeyed for part of the higher relative pressure range.

Figure 4 shows the kinetic profiles for methanol and ethanol adsorption on **M**. The kinetic models were considered a satisfactory fit for the normalized experimental data when the residuals from the calculated profile were within $<\pm 0.02$ for >95% of the experimental data. Typically, this gave a regression coefficient (R^2) of >0.99. It is evident that neither methanol nor ethanol adsorption on **M** follows the LDF model as observed previously for **E**. It is proposed that there are two barriers due to diffusion through the windows and along the pore cavities

(47) Loughlin, K. F.; Hassan, M. M.; Fatehi, A. I.; Zahur, M. *Gas Sep. Purif.* **1993**, *7*, 264.
(48) Crank, J. *The Mathematics of Diffusion*, 2nd ed.; Clarendon Press: Oxford, 1975.

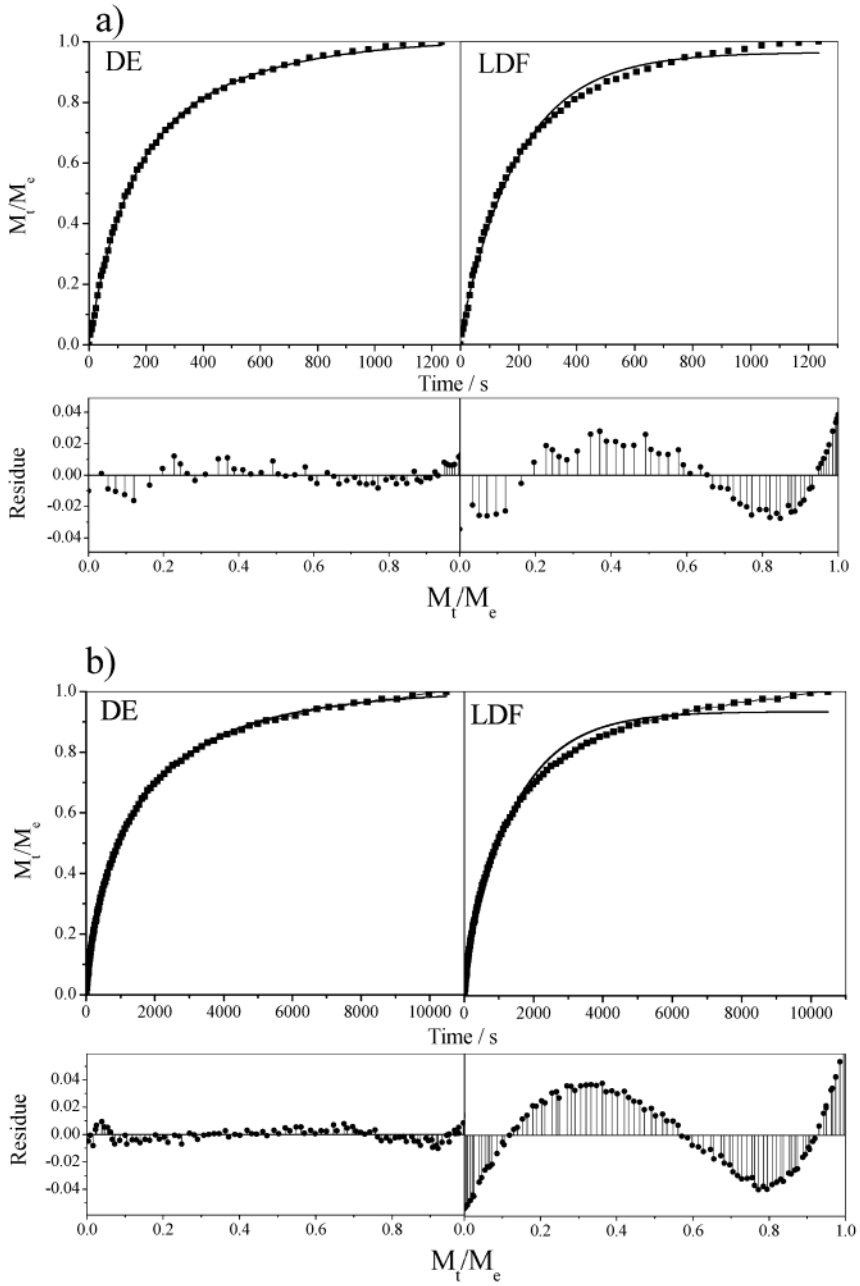

Figure 4. A comparison of adsorption kinetic profiles for M_t/M_e versus time for adsorption of methanol and ethanol on porous structure **M** and the fitting of the double exponential and linear driving force models to the experimental data: (a) methanol ($p/p^0 = 0.00098-0.00107$); (b) ethanol ($p/p^0 = 0.00957-0.01438$).

in the porous framework structures. This can be described by a double exponential (DE) equation:

$$M_t/M_e = A_1(1 - \exp(-k_1 t)) + A_2(1 - \exp(-k_2 t)) \quad (5)$$

where k_1 and k_2 are kinetic rate constants and A_1 and A_2 are the relative contributions of the two barriers controlling the overall process, with $A_1 + A_2 = 1$. Structural considerations indicate that the number of windows and pore cavities are equal and therefore the barriers should have equal fractional contributions giving $A_1 = A_2 = 0.5$. It is apparent that the kinetic profiles for both methanol and ethanol adsorption on **M** follow the DE model.

Methanol adsorption on **M** was studied over the temperature range 268−288 K in intervals of 5 K, whereas ethanol adsorption was studied at 273 and 298 K. Figure 5 shows a comparison of the rate constants for methanol adsorption at 288 K and ethanol adsorption at 298 K on porous structure **M** as a function of relative pressure. It is apparent that the rate constants increase with increasing relative pressure and all of the other temperatures studied show the same trends (see Supporting Information). This is the opposite trend to that observed for methanol and ethanol adsorption on **E**.[24] The rate constants for the fast and slow components for ethanol adsorption on **M** are slower than the corresponding steps for methanol adsorption despite the higher temperature for ethanol adsorption. This is consistent with the larger size of ethanol ($4.16 \times 4.27 \times 6.33$ Å) as compared to methanol ($3.81 \times 4.18 \times 4.95$ Å). When considering the diffusion of adsorptives into porous structures, one dimension is important for slit-shaped pores, whereas two

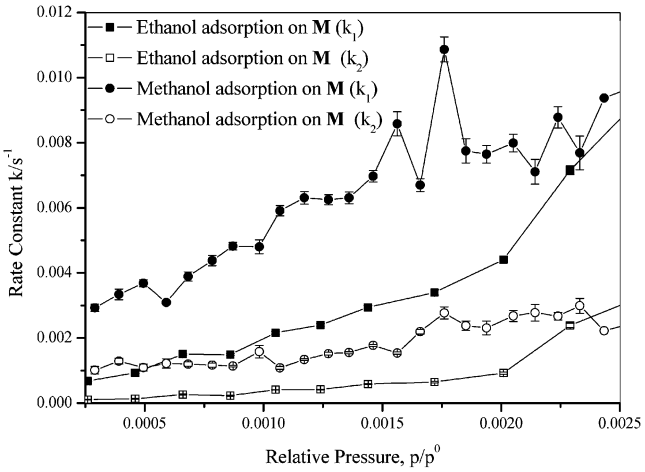

Figure 5. The variation of double exponential kinetic parameters k_1 and k_2 with relative pressure (p/p^0) for adsorption of methanol at 288 K and ethanol at 298 K on porous structure **M**.

dimensions are important for spherical pores. The relative order of the rate constants expected for ethanol and methanol adsorption is the same for both slit- and spherical-shaped pores.

X-ray Diffraction Measurements. Porous Structure E. Previous studies involved an investigation of the effect of methanol loading on the structural characteristics of **E**.[4] Figure 6 shows that the unit cell responds anisotropically with methanol loading as follows: the *a* and *c* cell parameters increase, while the *b* cell parameter decreases slightly. The expansion of the *a* cell dimension is of particular interest as this is the direction of the channels. The process of desolvation introduces disorder into the material on a length scale of ca. 100−500 Å. The X-ray data for 50% methanol loading show a small increase in the *c* dimension, but the *a* and *b* dimensions are unchanged within experimental error. The activation energies for adsorption obtained from the kinetic analysis using the LDF model increase slightly in this loading region (see Figure 6). However, the 240 and 113 reflections had a marked increase in peak width. As methanol loading increases, the peaks show a reduction in width, indicating an increase in order at high loadings. The volume occupied by a methanol molecule is ∼70% that of an ethanol molecule. The occurrence of the isotherm step at the point where two methanol molecules are located in the channels, precisely matching the loading of hydrogen-bonding guests to that in the as-grown structure templated around ethanol, suggests that the structure itself is optimized for the uptake of two hydrogen-bonding guests. Steric considerations influence site occupation above adsorption of two methanol molecules, and the structure is forced to readjust upon sorption of further guests. However, changes in the lattice parameters with methanol loading do not provide a clear indication of the isotherm step, but subtle changes in host structure may not be detectable.[4] The cell dimensions increase markedly above 75% loading and correspond to an increase of ∼2.6% in the unit cell volume at 100% loading.

The results reported here for ethanol adsorption on **E** show that the unit cell also responds anisotropically with ethanol loading. However, the *a* dimension decreases before increasing at high loading, while unit cell parameters *b* and *c* increase before decreasing slightly. The *b* and *c* dimensions correspond to the pore cross section. The unit cell volume increases sharply between 20% and 40% loading before reaching a plateau. This

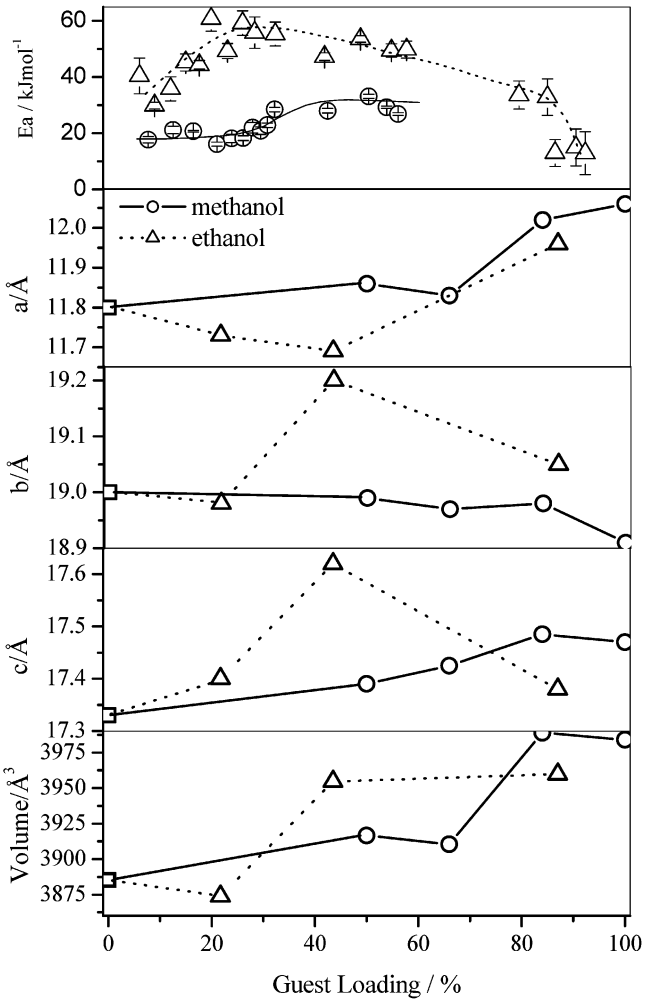

Figure 6. A comparison of the variation of activation energies for methanol (○) and ethanol (△) adsorption derived from LDF kinetic parameters,[4] unit cell dimensions *a*, *b*, and *c*, and unit cell volume for porous structure **E** as a function of guest loading: methanol (○) and ethanol (△).

expansion corresponds to an increase of ∼1.8% in the unit cell volume. This expansion at low loading contrasts with the other cases of cell expansion during adsorption, which occur after ∼75% loading. It is apparent that the scissoring motion resulting from ethanol loading is quite different from that produced by methanol sorption. The marked change in cell parameters and unit cell volume at 40% loading coincides with the broad peak in ethanol adsorption kinetic activation energies (see Figure 6). Therefore, the change in unit cell parameters and unit cell volume can be linked to changes in the barriers to diffusion into the porous structure. At higher loadings, there is further structural relaxation with an increase in the *a* dimension, that is, along the direction of the pore array. This coincides with a decrease in the activation energies for diffusion into the porous structure. The structural changes during the adsorption process affect the diffusion of guests into the porous structure.

Porous Structure M. Figure 7 shows that the unit cell responds anisotropically with methanol loading as follows: the *b* and *c* cell parameters increase, while the *a* cell parameter decreases slightly. The unit cell volume increases sharply after ∼70% loading. The unit cell at 100% loading is approximately 2.9% larger than the desolvated porous structure in a vacuum. The scissoring motion of the structure occurs to expand the volume without affecting the bond lengths significantly.

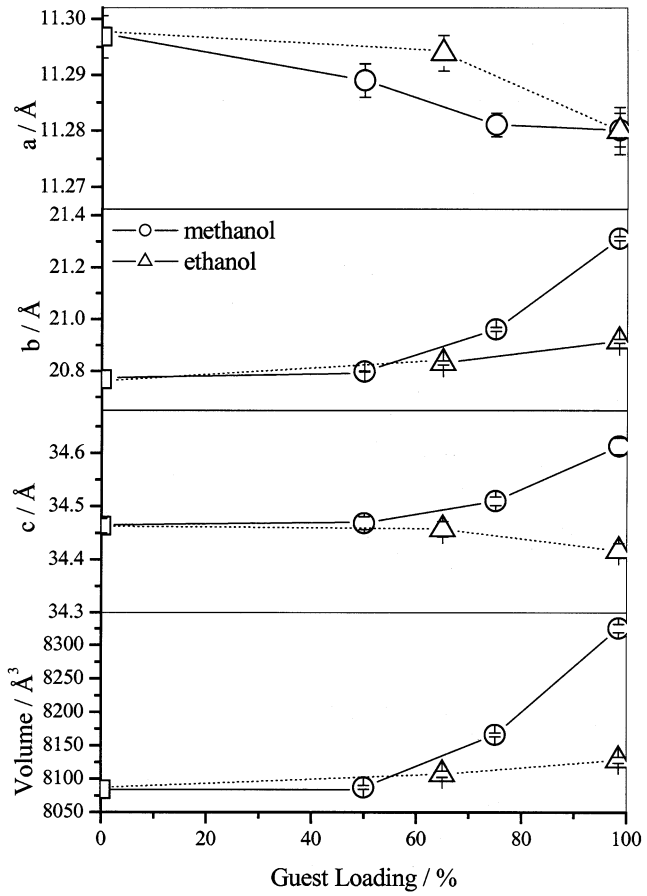

Figure 7. The variation in lattice parameters *a*, *b*, and *c* and unit cell volume for porous structure **M** as a function of methanol and ethanol loading. Symbols for the parameters are as follows: desolvated material (□), CH_3OH loadings (○), and C_2H_5OH loadings (△).

Adsorption of ethanol on **M** is different from the corresponding adsorption of methanol. First, the amount of ethanol adsorbed at $p/p^0 = 1$ was 2.42 mmol g^{-1}, whereas the uptake for methanol at $p/p^0 = 1$ was 4.48 mmol g^{-1}. The ethanol molecules have only 50% occupancy of the surface oxygen sites of the nitrates. The volume occupied by a methanol molecule is ~70% that of an ethanol molecule. Hence, it is apparent that the available pore volume is only ~78% filled by the ethanol molecules at $p/p^0 = 1$, indicating the presence of voids in the porous structure. The X-ray diffraction data also reflect the incomplete filling of the pore structure. The unit cell responds anisotropically with ethanol loading as follows: the *a* and *c* cell parameters decrease slightly, while the *b* parameter increases slightly. The unit cell volume increases slightly by 0.4%, which is much smaller than for methanol adsorption (2.9%). The lack of expansion of the unit cell is consistent with voids in the pores and incomplete filling of **M** by the ethanol adsorbate.

Adsorption Dynamics. Rao *et al*. developed a model[49,50] for the interaction potential of diffusing species in porous carbons and concluded that two processes are involved: (a) diffusion along the pores; and (b) diffusion through the barrier at the pore entrance. A LDF model is followed when the latter is the rate-determining step, and a Fickian diffusion model is followed when the former controls the kinetics. When both processes are significant, a combined barrier resistance/diffusion model is followed. This has been observed for adsorption of a wide range of adsorptives on porous carbons.[32−38] Previous studies of the diffusion of carbon dioxide into a carbon molecular sieve have shown that the mechanism changes from LDF through combined barrier resistance/diffusion to Fickian diffusion, with changes in adsorption temperature and pressure.[33]

The Darken equation has been used to describe the variation of diffusivity (D) with surface coverage (θ), and in the case of a system obeying the Langmuir isotherm the following relation has been derived:[51,52]

$$D_\theta/D_0 = 1/(1 - \theta) \qquad (6)$$

where D_θ and D_0 are the diffusivities at θ and zero surface coverage, respectively. This implies that the diffusivities increase with increasing surface coverage and a graph of $1/D_\theta$ versus θ or amount adsorbed (n/mmol g^{-1}) should give a straight line. The diffusion coefficient D is directly proportional to the rate constant, k.

The Langmuir isotherm has the following form:

$$p/n = 1/n_m b + p/n_m \qquad (7)$$

where p is the pressure, n is the amount adsorbed, n_m is the monolayer capacity, and b is the coefficient of adsorption specific to the adsorbate/adsorbent system.[1] The Langmuir isotherms for adsorption of ethanol on **M** gave maximum amounts adsorbed of 1.821 ± 0.007 mmol g^{-1} ($R = 0.99983$) at 273 K and 1.826 ± 0.003 mmol g^{-1} ($R = 0.99996$) at 298 K.

Ethanol adsorption isotherms for both **M** and **E**[4] follow the Langmuir isotherm but have opposite trends for kinetic parameters with surface coverage. Previous studies have shown that the LDF rate constants for ethanol adsorption on **E** decrease with increasing relative pressure, reaching a minimum at $p/p^0 = \sim 0.009$ (~50% pore volume), and increase thereafter up to >90% pore filling before the kinetic model changes to a combined barrier resistance/diffusion model. This trend is contrary to that expected from the Darken equation. In contrast, for adsorption of ethanol on **M**, in the initial uptake region, both rate constants obtained from the DE model increase with increasing surface coverage. Figure 8 shows that graphs of reciprocal of DE rate constants k_1 and k_2 versus amount adsorbed (n/mmol g^{-1}) for ethanol adsorption on **M** are linear. Therefore, the kinetic data are consistent with the prediction of the Darken equation. The reason for ethanol adsorption **E** not following the Darken equation is probably the marked structural change during sorption at low guest loading involving the scissoring motion, which is much smaller for ethanol adsorption on **M** (see Figures 6 and 7). In both cases, the mechanism involves adsorption of methanol or ethanol molecules on oxygen surface sites by hydrogen bonding. Therefore, the different kinetic trends are related to differences in porous structures **M** and **E**.

The adsorption kinetics for methanol adsorption on **M** were measured over the temperature range 268−288 K. Activation energies for both the fast and the slow DE rate constants were calculated. Figure 9 shows the variation of the activation

(49) Rao, M. B.; Jenkins, R. G.; Steele, W. A. *Ext. Abstr. Program − Biennial Conf. Carbon* **1985**, 114.
(50) Rao, M. B.; Jenkins, R. G.; Steele, W. A. *Langmuir* **1985**, *1*, 137.
(51) Yang, R. T. *Gas Separation by Adsorption Processes*; Butterworths: Boston, 1987.
(52) Kapoor, A.; Yang, R. T.; Wong, C. *Catal. Rev. Sci. Eng.* **1989**, *31*, 129.

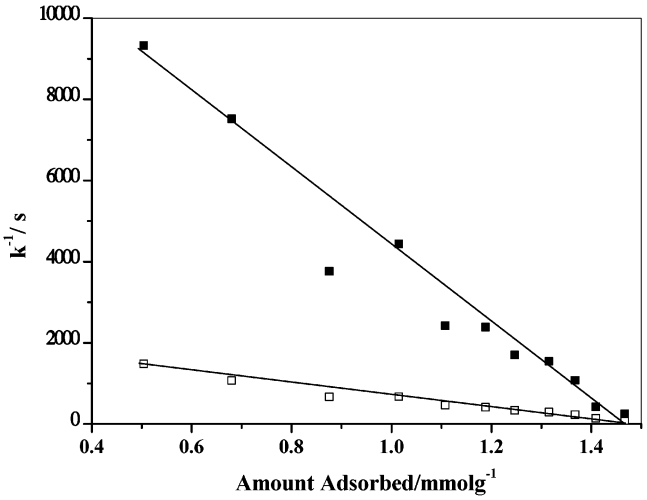

Figure 8. The variation of the reciprocal of double exponential rate constants k_1 (□) and k_2 (■) with the amount adsorbed for ethanol adsorption on porous structure **M** at 298 K.

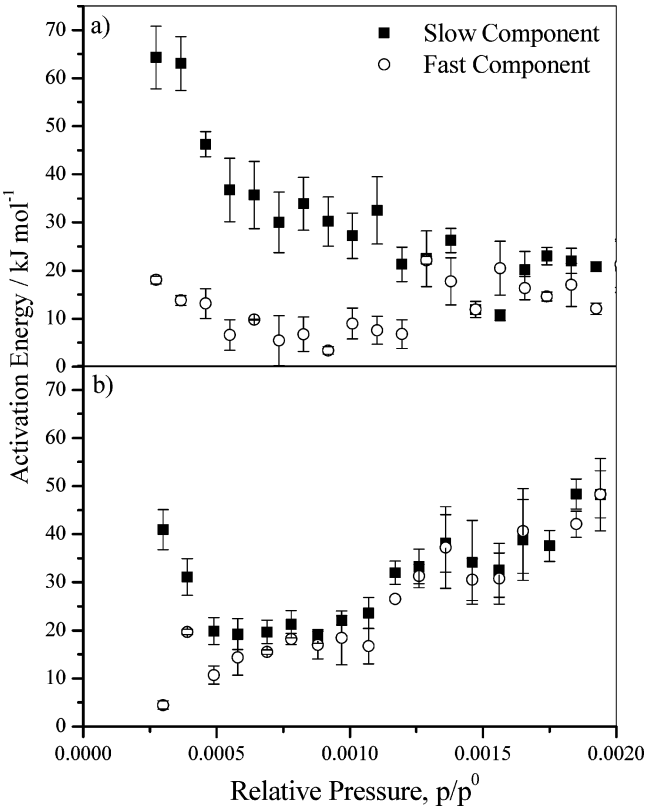

Figure 9. The variation of activation energy with relative pressure for methanol adsorption on (a) porous structure **M** over the temperature range 268−288 K and (b) porous structure **E** over the temperature range 273−293 K.

energies as a function of relative pressure. In the initial uptake region (0.15 mmol $g^{-1} < n$), the slow component has a high activation energy (56−64 kJ mol^{-1}), while the fast component has a low activation energy (13−18 kJ mol^{-1}). The differences in the activation energies for the two components decreases with increasing relative pressure and converge at $p/p^0 \approx 0.0013$ ($n = 0.4$ mmol g^{-1}, 0.016 cm^3 g^{-1}) with average activation energies of 18.2 ± 2.4 and 15.4 ± 7.1 kJ mol^{-1} for the slow and fast components for pressure increments 20−26, respectively. This is an example of cooperative effects where increasing adsorption induces structural changes, which decrease the barrier due to the windows in the porous structure, while the barrier due to diffusion through the pore cavities increases slightly so that the kinetic barriers are similar at high surface coverage. The results from previous studies of methanol adsorption on **E** were reanalyzed using the DE model, and the results are shown in Figure 9b. It is apparent that only the first three pressure increments show clear differences in the activation energies of the two components. The activation energies for the rest of the pressure increments were not significantly different, that is, for virtually all of the kinetic data. Therefore, the original kinetic analysis using a linear driving force model is appropriate. However, there is the suggestion from the first three pressure steps of the resolution of two barriers to diffusion of methanol into **E**. While this evidence alone is not conclusive for the resolution of the two kinetic barriers, it provides support for resolution of the two kinetic barriers for adsorption of methanol on **M**. It is apparent that the barriers to diffusion through the windows and pores can be resolved at low loading, but they merge at high loading due to cooperative effects and structural change.

The kinetic data for ethanol adsorption on **E** could not be resolved into two kinetic barriers. Previous studies of the adsorption LDF rate constants and activation energies for ethanol adsorption on **E**, as a function of surface coverage, show that the minimum in the rate constant occurs at 50% total pore volume ($p/p^0 \approx 0.009$), while the maximum activation energy occurs at $p/p^0 \approx 0.0015-0.003$ (20−40% total pore volume or loading). There is only a small change in activation energy up to 50% total pore volume, above which it decreases markedly. Methanol adsorption on **E** also shows a slight decrease in rate constant with increasing p/p^0. The activation energies for adsorption of ethanol (10−60 kJ mol^{-1}) are much higher than for methanol adsorption (16−33 kJ mol^{-1}) on **E** at the same loading. This may be attributed to the larger minimum dimensions of ethanol as compared to those of methanol.[44,45]

The activation energies for adsorption of methanol on **M** for the fast (k_1) and slow (k_2) DE components are in the ranges 4−24 and 15−64 kJ mol^{-1}, respectively. Graphs of ln(pre-exponential factor) and activation energy (Ea) for these data are compared to the corresponding data obtained from LDF kinetic parameters for methanol and ethanol adsorption on **E** in Figure 10. The individual graphs overlap and are linear. Graphs of ln(k) versus $1/T$ for all of the adsorption systems converge to well-defined isokinetic points with nonzero isokinetic rates.[4,34,37,38] This is consistent with a compensation effect for both DE components.

Previous studies have shown that the adsorption of a wide range of adsorptives varying from water to *n*-nonane, thereby ranging from hydrophilic to hydrophobic character, on active carbon, follow a compensation effect.[34,37,38] This was attributed to a mechanism where a high barrier results in build-up of the adsorptive in front of the barrier, leading to an increased pre-exponential factor and vice versa.

Adsorption Kinetics in Relation to Structural Change. X-ray diffraction data show that both **M** and **E** undergo scissoring motions, which are nonlinear with adsorption of both methanol and ethanol guest molecules. This involves hydrogen bonding to specific nitrate oxygen surface sites and may be driven by increased ordering of the adsorbate molecules and

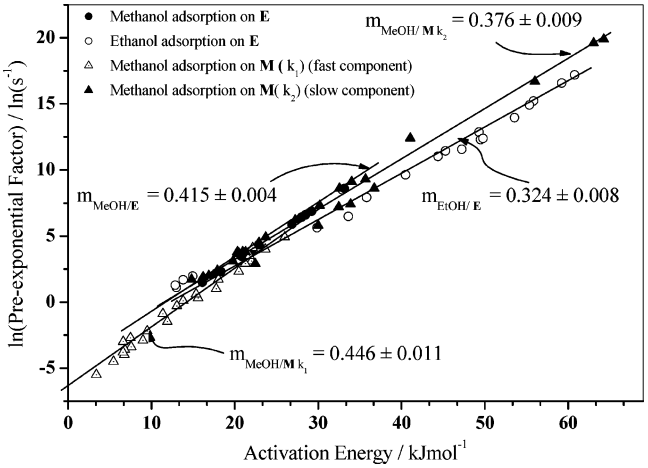

Figure 10. A comparison of the variation of ln(pre-exponential factor) (ln(*A*)) with activation energy (Ea) for methanol (●) and ethanol (○) on porous structure **E** derived from LDF kinetic parameters[24] and methanol, fast component k_1 (△) and slow component k_2 (▲) on porous structure **M** derived from kinetic analysis using the double exponential model.

adsorbate/adsorbate interactions with increasing adsorbate density in the channels. The availability of both void volume and the presence of a specific number of guest binding sites may control guest uptake in flexible molecular frameworks. The total pore volumes obtained from ethanol and methanol adsorption isotherms for **E** were similar. However, the methanol adsorption isotherm is quite different and has a step at approximately 70% pore volume, corresponding to sorption of two molecules of methanol per dimer unit. This step is indicative of a structural rearrangement of the host structure, to allow further methanol adsorption on additional sites to those sites occupied in the material fully loaded with ethanol. The three methanol molecules sorbed per Ni_2(4,4′-bipyridine)$_3(NO_3)_4$ structural unit in **E** demonstrates that pore filling occurs. In contrast, the adsorption of a maximum of two molecules of ethanol per dimer unit of **M** indicates incomplete pore filling and the importance of adsorbate/adsorbent interactions. Previous examples of adsorption systems where Gurvitch's rule is not obeyed have been attributed to activated diffusion and size exclusion effects. As far as we are aware, this is the first case where it is directly attributable to specific adsorbate−adsorbent interactions.

The activation energies for diffusion of ethanol into **E** increase with increasing amount adsorbed followed by a marked decrease in the activation energy after 50% pore filling. This coincides with structural relaxation by a scissoring motion along the axis of the linear array of pores as shown by the X-ray structure measurements. However, there is disorder in the unidentate and bidentate nitrate ions. This may also be a factor in the marked change in activation energy at 50% pore volume.

Conclusions

Methanol and ethanol adsorption on both porous structures **E** and **M** formed by desolvation of Ni_2(4,4′-bipyridine)$_3(NO_3)_4$•$2C_2H_5OH$ and Ni_2(4,4′-bipyridine)$_3(NO_3)_4$•$2CH_3OH$, respectively, induces scissoring movements with two cell dimensions increasing and the third decreasing, but the unit cell space groups remain unchanged. The structural changes for ethanol adsorption on **M** are much smaller than the others because they are limited by specific adsorbate/adsorbent interactions, leaving voids in the porous structure so that complete pore filling does not occur. In the case of methanol adsorption on **E**, once the nitrate sites are occupied, the adsorbent undergoes a structural change, resulting in an isotherm step associated with a marked slowing in the adsorption kinetics, to accommodate further methanol.

The adsorption of methanol and ethanol on **M** follows a double exponential model with equal contributions from two diffusion barriers due to windows and pore cavities in the flexible porous framework structure. In the initial uptake regions, the activation energies derived from the two kinetic processes for diffusion through the windows and pore cavities are a slow component with a high activation energy (∼60 kJ mol^{-1}) and a fast component having a low activation energy (∼15 kJ mol^{-1}), respectively. The differences in activation energy converge at higher relative pressure due to cooperative effects inducing structural change. Previous studies showed that the kinetic barriers for methanol adsorption on **E** were similar and could not be resolved into individual components for all but three steps in the initial uptake region. The activation energies for adsorption of ethanol (10−60 kJ mol^{-1}) and methanol (16−33 kJ mol^{-1}) on **E** are comparable to those obtained for methanol adsorption on **M**. The kinetic data for both **M** and **E** follow a similar compensation effect. The differences can be attributed to the size of the adsorptives in relation to the adsorbent structural barriers. The maximum in the activation energies for ethanol adsorption on **E** occurs at ∼40% loading, where a scissoring motion results in expansion of the cell volume leading to lowering of activation energy for diffusion into the porous structure. It is apparent that structural characteristics and induced structural changes during loading are closely related to adsorption thermodynamic and kinetic characteristics.

Acknowledgment. We would like to thank Dr. C. E. Webster of Texas A&M University and the late Dr. M. C. Zerner of the University of Florida for providing additional calculations of the adsorptive dimensions for methanol and ethanol.

Supporting Information Available: Langmuir isotherms and kinetic data. Crystallographic information in CIF format. This material is available free of charge via the Internet at http://pubs.acs.org.

JA0490267